

# Full-Wave Feasibility Study of Anti-Radar Diagnostic of Magnetic Field Based on O-X Mode Conversion and Oblique Reflectometry Imaging

Orso Meneghini<sup>1</sup> and Francesco A. Volpe<sup>2, a)</sup>

<sup>1)</sup>General Atomics, San Diego, California, USA

<sup>2)</sup>Dept of Applied Physics and Applied Mathematics, Columbia University, New York, New York USA

An innovative millimeter wave diagnostic is proposed to measure the local magnetic field and edge current as a function of the minor radius in the tokamak pedestal region. The idea is to identify the direction of minimum reflectivity at the O-mode cutoff layer. Correspondingly, the transmissivity due to O-X mode conversion is maximum. That direction, and the angular map of reflectivity around it, contain information on the magnetic field vector  $\mathbf{B}$  at the cutoff layer. Probing the plasma with different wave frequencies provides the radial profile of  $\mathbf{B}$ . Full-wave finite-element simulations are presented here in 2D slab geometry. Modeling confirms the existence of a minimum in reflectivity that depends on the magnetic field at the cutoff, as expected from mode conversion physics, giving confidence in the feasibility of the diagnostic. The proposed reflectometric approach is expected to yield superior signal-to-noise ratio and to access wider ranges of density and magnetic field, compared with related radiometric techniques that require the plasma to emit Electron Bernstein Waves. Due to computational limitations, frequencies of 10-20 GHz were considered in this initial study. Frequencies above the edge electron-cyclotron frequency ( $f > 28$  GHz here) would be preferable for the experiment, because the upper hybrid resonance and right cutoff would lie in the plasma, and would help separate the O-mode of interest from spurious X-waves.

PACS numbers: 52.35.Hr, 52.70.Gw, 52.55.-s, 07.60.Hv

## I. INTRODUCTION AND PHYSICAL PRINCIPLE

Internal measurements of magnetic field and current density in a tokamak are important but notoriously difficult<sup>1-5</sup>. The present numerical work addresses the feasibility of an innovative millimeter wave diagnostic, which is expected to measure the local magnetic field vector  $\mathbf{B}$  as a function of the minor radius in the pedestal region. As such, it could complement Motional Stark Effect polarimetry<sup>6,7</sup>, characterized by good signal-to-noise in the plasma core.

The physical principle, illustrated in Figs.1,2, is as follows. An angularly broad mm-wave beam of ordinary (O) polarization is obliquely injected in the magnetized plasma; at the O-mode cutoff layer, part of the incident wave converts in the extraordinary (X) mode with conversion efficiency<sup>8</sup>

$$C = \exp \left\{ -\pi k_0 L \sqrt{\frac{Y}{2}} \left[ 2(1+Y)(N_{z,opt} - N_z)^2 + N_y^2 \right] \right\} \quad (1)$$

and transmits through the cutoff layer. Here  $L$  is the length scale of density non-uniformity and  $Y = \Omega_e/\omega$  the dimensionless magnetic field at the cutoff location  $X = 1$ , where  $X = \omega_{pe}^2/\omega^2$  is the dimensionless density and  $\Omega_e$ ,  $\omega_{pe}$  and  $\omega$  are respectively the electron cyclotron, plasma and wave frequencies. The conversion efficiency is maximum for incidence in the plane spanned by the density gradient (assumed in the  $x$  direction) and magnetic field

(pointing in the  $z$  direction) with an optimal  $z$  component of the refractive index,  $N_{z,opt} = \sqrt{Y/Y+1}$ , with  $Y$  evaluated at the  $X = 1$  location.

The rest of the wave keeps the original O-mode polarization and is reflected by the O-mode cutoff with angle-dependent reflectivity  $1 - C$ . From Eq.1 it follows that  $1 - C$  contains information on the magnetic field strength (through  $Y$ ). It also contains information on the field orientation, because the plane  $y - z$  is spanned by the density gradient (basically, the minor radius direction) and the magnetic field, therefore its inclination in the laboratory frame is the same as the magnetic pitch angle. Both pieces of information are evaluated at the cutoff layer for the frequency considered. That is, the diagnostic is internal and local. The angle-dependent reflectivity can be measured using a single launcher and an array of receivers. In some sense the diagnostic can be considered an “anti-radar” that identifies and characterizes minima, rather than maxima, of reflectivity. Finally, *frequency-resolved* measurements of reflectivity provide *radially* resolved measurements of magnetic field strength and pitch angle.

A related, earlier technique relies on partial transmission, though the O-mode cutoff, of internally emitted electron Bernstein (B) waves (EBW) undergoing BXO mode conversion<sup>9-11</sup>. However, not all fusion plasmas are over-dense EBW emitters. The new technique proposed here overcomes this limitation and is applicable whenever reflectometry is applicable. Furthermore, the signal to noise ratio is higher, by simply adopting a sufficiently intense reflectometric source. The spatial and temporal resolution are comparable with other reflectometric imaging systems<sup>12-14</sup>.

<sup>a)</sup>Corresponding author: fvolpe@columbia.edu

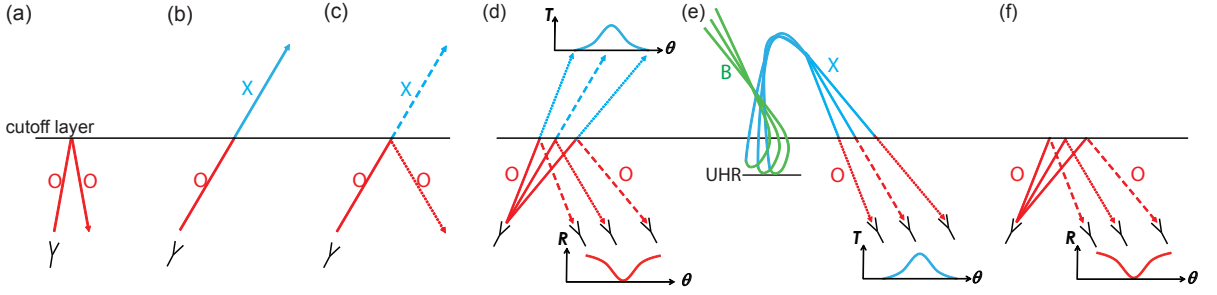


FIG. 1. Physical principle, single ray: (a) cutoff layer ( $\omega = \omega_{pe}$ ) is fully reflective for a perpendicular O-mode beam (red), but (b) fully transmissive for an oblique O-mode of special inclination, dependent on local  $|\mathbf{B}|$ . Full transmission is due to full conversion into X-mode<sup>8</sup>. (c) Oblique beam of near-optimal inclination is partly reflected, partly transmitted. Bundle of rays: (d) A wide-angle beam experiences a peak in O-mode transmissivity  $T$  and consequently a hole in O-mode reflectivity  $R$ . The anisotropy of  $R$  depends on the local vector  $\mathbf{B}$ , not solely on  $|\mathbf{B}|$ . (e) Angular peaks of BXO conversion efficiency have been observed in plasmas emitting EBWs<sup>9–11</sup>. (f) A peak in OX conversion efficiency of an externally launched O-mode and, consequently, a hole in O-mode reflectivity, are expected in any device where reflectometry is possible. Here dashed and dotted lines denote respectively rays of low and high intensity, due to partial transmission or reflection.

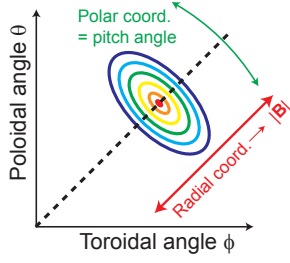


FIG. 2. Position and orientation of reflectivity contours (plotted as functions of view angles) are indicative of  $\mathbf{B}$  strength and direction at O-mode cutoff, respectively.

## II. FULL-WAVE SLAB MODEL

To validate this physical principle, we performed preliminary simulations using the COMSOL Multiphysics code and its RF module<sup>15</sup>. The code uses Finite Element Method to solve arbitrary sets of partial differential equations. The RF module enables solution of Maxwell's equations in media characterized by anisotropic complex dielectric tensors with spatial variations in 1D, 2D and 3D. This software has been used and benchmarked for solving the problem of antenna-plasma wave coupling and wave propagation in cold plasmas, as reported in Ref.<sup>16</sup>. Warm plasma effects would be needed to model the BXO conversion used in radiometric techniques<sup>9–11</sup>, but not for the OX conversion invoked here.

Figure 3 illustrates the slab geometry chosen for this study. Notice the two sets of Cartesian coordinates. All plasma parameters vary only in the  $x$  direction, playing the role of the radial coordinate. The magnetic field points in the  $\hat{z}$  direction, and the wave vector  $\mathbf{k}$  forms an angle  $\theta$  relative to it.  $E_{\theta p}$  and  $E_{\phi p}$  are wave field components parallel and perpendicular to the plane spanned by  $\hat{x}$  and  $\hat{z}$ . From the cold plasma dispersion relation, it follows that the ellipticity of the O-mode polarization is

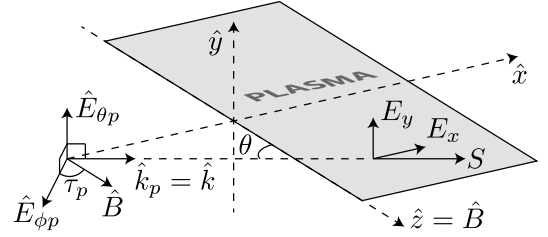


FIG. 3. Definition of a set of Cartesian coordinates  $\hat{x}, \hat{y}, \hat{z}$  in the plasma slab and of an additional set of coordinates, rotated to align one of its axes to the wave-launch direction.

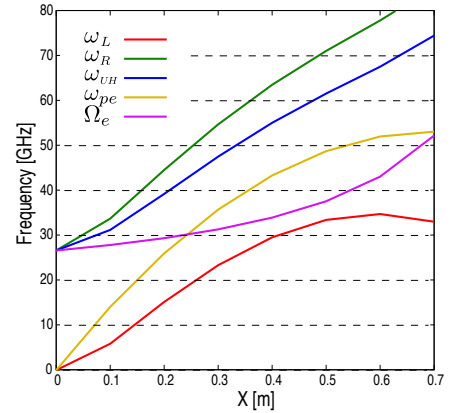


FIG. 4. Cutoff and resonant frequencies as a function of the  $\hat{x}$  coordinate.

given by<sup>17</sup>:

$$\frac{E_{\phi p}}{E_{\theta p}} = \left[ \frac{2i \sin \tau_p}{Y \cos^2 \tau_p + \sqrt{(Y \cos^2 \tau_p)^2 + 4 \sin^2 \tau_p}} \right] \quad (2)$$

where  $\tau_p$  is the angle that  $E_{\phi p}$  forms relative to the magnetic field or, equivalently, relative to  $\hat{z}$ .

In the slab in Fig.3,  $x=0$  corresponds to the plasma edge on the low-field side, and  $x=0.7$  m corresponds to the plasma center. The magnetic field evaluates 1.9 T at the plasma center, and decays like  $1/(R+a-x)$ , where  $R=0.78$  m and  $a=0.7$  m. The electron density is modeled as  $n_e = n_{e0} [1 - (1 - x/a)^2]^2$ , with  $n_{e0} = 3.5 \times 10^{19} \text{ m}^{-3}$ .

Fig.4 shows the corresponding profiles of left cutoff  $\omega_L$ , right cutoff  $\omega_R$ , upper hybrid resonance  $\omega_{UH}$ , electron plasma frequency  $\omega_{pe}$  and electron cyclotron frequency  $\Omega_e$ . The figure refers to perpendicular launch ( $\theta = 90^\circ$ ). It should be noted that the radial locations satisfying  $\omega = \omega_L$  and  $\omega = \omega_R$  vary with  $\theta$ , as it will be clearly visible in Fig. 5.

The minimum requirement for this technique is that the O-mode cutoff layer defined by  $\omega = \omega_{pe}$  lies in the plasma for the  $\omega$  of choice, so that the O-X conversion can occur. For the frequencies adopted here ( $\omega/2\pi=10$ -20 GHz), a wave launched perpendicularly to the plasma at  $x=0$  encounters the plasma cutoff and the left cutoff (yellow and red in Fig.4). At higher frequencies,  $\omega/2\pi > \Omega_e(x=0)/2\pi=28$  GHz, the wave will cross the  $\omega = \omega_R$  X-mode cutoff and the the upper hybrid resonance before reaching the O-mode cutoff. At higher frequency, above the maximum plasma frequency  $\omega_{pe0}$  (calculated using  $n_{e0}$ ), no O-mode cutoff is present in the plasma, no O-X conversion occurs, and the technique is not applicable.

Note that the O-mode is only sensitive to the  $\omega = \omega_{pe}$  cutoff, and the X-mode is only sensitive to the left and right cutoff and to the upper hybrid resonance. The technique relies on the oblique injection of an O-mode, and its partial conversion in a slow X-mode. The mode conversion occurs at the evanescent layer between the  $\omega = \omega_{pe}$  and the  $\omega = \omega_L$  locations. In practice, though, the injected polarization is rarely a pure O-mode, implying that some amount of fast X-mode is also injected. As a consequence, all cutoffs and resonances need to be taken into account in interpreting the complex wave-fields that will be discussed in the next Section.

### III. SIMULATION RESULTS

In our study we investigated the wave launch, propagation and reflection at the cutoff layers for different values of the injection angle  $\theta$  and of the wave frequency  $f = \omega/2\pi$ . Because of limitations in the present computational resources, in this initial paper we studied frequencies, 10-20 GHz, reflected at the very edge of the plasma. Extension to the 30-75 GHz range, corresponding to cutoff densities  $n_e=1-7 \times 10^{19} \text{ m}^{-3}$ , and thus more relevant to a tokamak pedestal, is left as a future work.

Fig. 5 shows contours of the magnitude  $|\mathbf{E}|$  of the wave electric field for  $f = 10 \text{ GHz}$  and  $\theta = 30^\circ$  and  $f = 20 \text{ GHz}$  and  $\theta = 50^\circ$ . In our model the incident wave power is distributed uniformly at the antenna mouth, with a wave field polarization as from Eq. 2. After propagating in vacuum, the waves reach the plasma edge ( $x = 0$ ,  $n_e = 0$ ). From there, the O-mode and X-

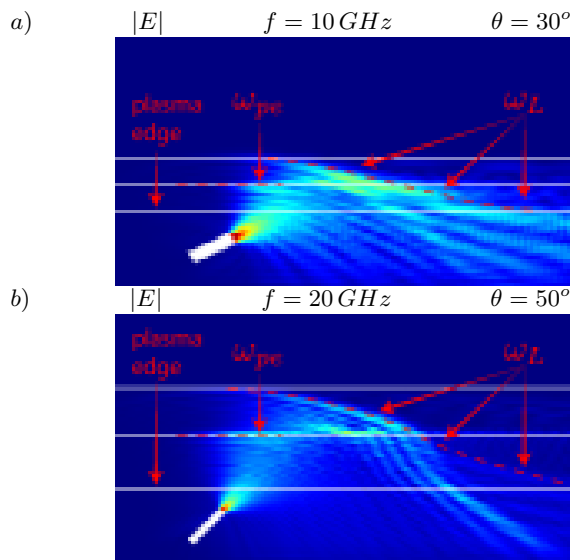


FIG. 5. Magnitude of the total electric field for (a)  $f = 10 \text{ GHz}$  and  $\theta = 30^\circ$  and (b)  $f = 20 \text{ GHz}$  and  $\theta = 50^\circ$ . The three horizontal white lines represent the plasma edge, the O-mode cutoff ( $\omega = \omega_{pe}$ ) and the location where  $\omega = \omega_L|_{\theta=90}$ . The simulation domain extends 1 m and 0.4 m in the  $\hat{z}$  and  $\hat{x}$  directions, respectively.

mode (if any) propagate until they reach, respectively, the  $\omega = \omega_{pe}$  and the outermost between the  $\omega = \omega_R$  and  $\omega = \omega_L$  layer. As discussed before, at the low frequencies examined here, only the  $\omega = \omega_L$  layer exists in the plasma (Figs.4,5), but note that the actual turning point can lie slightly past it<sup>18</sup>. In the region between the O-mode and X-mode cutoff, only the X-mode wave can propagate. In these figures, ripples in the wave fields magnitude indicate wave interference which is symptomatic of wave reflection at the aforementioned layers.

Figure 6 shows the magnitude of the wave electric field, as computed along the plasma edge ( $x = 0$ ) for various  $\theta$  and  $f$ . This simulation is representative of what an array of receivers could measure, as a function of  $z$ . A peak is detected at  $z < 0.4$  m (that is, close to the launcher), especially for large values of  $\theta$ , when launch is nearly perpendicular to the plasma. This peak is partly due to waves that, from the launcher, directly reach the receivers without any interaction (reflection, mode conversion) with the O-mode cutoff. To avoid this, in the actual diagnostic the receivers will be placed in a retracted position, at larger minor radii compared with the launching antenna.

The wave fields shown in the ranges of  $0.4 < z < 1.0$  m are mostly representative of the reflected waves at both  $\omega = \omega_{pe}$  and  $\omega = \omega_L$  layers. As mentioned above, there is no right-hand cutoff layer in the plasma for  $f = 10 \text{ GHz}$  and  $20 \text{ GHz}$ , and reflection of the X-mode is due to the L cutoff.

Figure 7 illustrates more details for the propagation and reflection of each component of the incident RF wave electric field for the case of  $f = 10 \text{ GHz}$  at  $\theta = 30^\circ$ . The

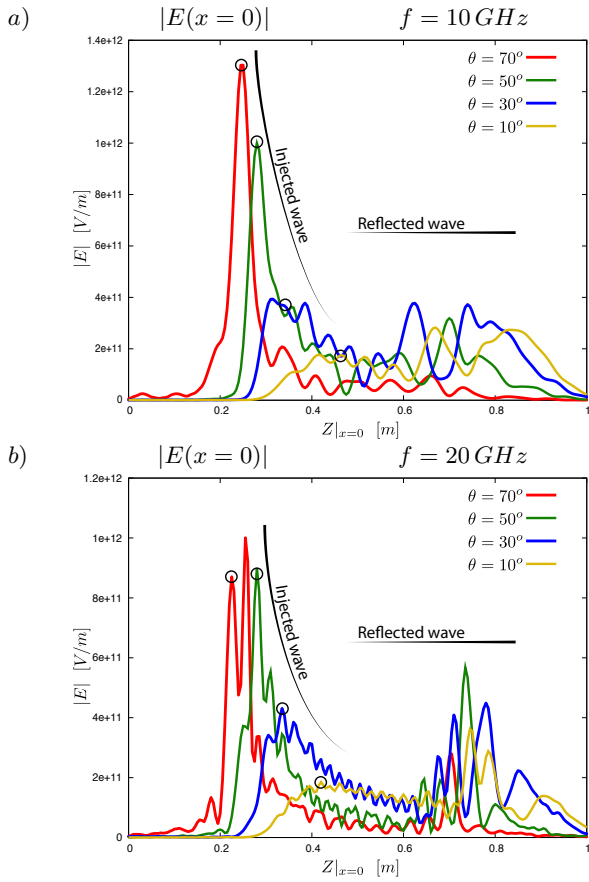


FIG. 6. Magnitude of the RF wave electric field computed along the plasma edge ( $x = 0$ ) for  $\theta = 70^\circ, 50^\circ, 30^\circ, 10^\circ$  at  $f = 10 \text{ GHz}$  and  $20 \text{ GHz}$ . The electric field for  $x < 0.4 \text{ m}$  is mostly representative of the waves launched by the antenna, while the values for  $x > 0.4 \text{ m}$  are mostly affected by the waves which are reflected at both  $\omega = \omega_{pe}$  and  $\omega = \omega_L$  layers.

O-mode ( $E_z$ ) propagates in the plasma, and then is cutoff at  $\omega = \omega_{pe}$  and reflected back to the plasma boundary. The X-mode ( $E_y$ ) propagates up to the left cutoff layer and is then reflected towards the plasma boundary. Similar results were obtained for  $f = 20 \text{ GHz}$  at  $\theta = 50^\circ$ .

These COMSOL calculations in simplified slab plasma geometry take only few minutes on a desktop computer. For higher frequencies (thus, shorter wavelengths), the mesh needs to be refined, resulting in longer cpu times. The main limitation, however, is posed by the large memory requirements.

#### IV. DISCUSSION, CONCLUSIONS AND FUTURE WORK

This study offers a preliminary outlook towards the possibility of reflectometrically measuring the magnetic field  $\mathbf{B}$  at the O-mode cutoff layer. As discussed in connection with Eq.1 and Fig.2, the information on the magnetic pitch angle is contained in the inclination of the

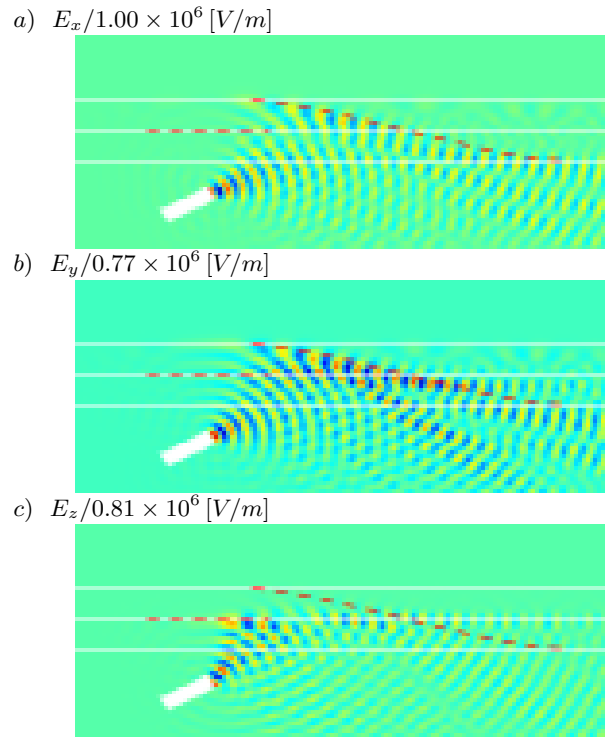


FIG. 7. Individual components of the waves total electric field a)  $E_x$ ; b)  $E_y$ ; c)  $E_z$  for  $f = 10 \text{ GHz}$  at  $\theta = 30^\circ$ . Absence of the  $E_z$  component indicates X-mode propagation. From this figure it is clear that the wave fields at the plasma edge ( $x = 0$ ) are a superposition of the reflections occurring at the O-mode and L-mode cutoff layers

angular contours of reflectivity, and the information on  $|\mathbf{B}|$  is contained in the special direction yielding maximum OX conversion efficiency, hence minimum reflectivity of the O-mode. Full-wave simulations exhibited the expected “hole” in reflectivity for that special direction of incidence. At the frequencies analyzed in our study (10-20 GHz), simulations show also that this reflectivity hole is complicated by reflections at the X-mode cutoff layer, which is itself a function of the the angle of incidence.

For frequencies higher than the electron cyclotron frequency as evaluated at the outer boundary,  $\omega > \Omega_e(x = 0)$ , the right-hand cutoff and upper hybrid (UH) resonance will be present in the plasma. The cutoff will reflect power accidentally injected in the X-mode. Furthermore, the UH resonance and the evanescent layer lying between it and the R cutoff will nearly entirely prevent the X-mode generated by the OX conversion from reaching the receivers outside the plasma. In other words, the R cutoff and UH resonance would “sanitize” the diagnostic scheme from fast X and slow X-mode waves, respectively, and the receivers would only (or mostly) detect the reflected O-mode of interest.

In that case, wave propagation shares similarities with EBW emission diagnostics based on the BXO mode conversion. Yet, the anti-radar diagnostic will offer the advantages of being an active diagnostic and not relying on

the plasma to be over-dense and to be an intense EBW emitter with good B-X conversion efficiency. Future simulations at high frequency will be necessary to confirm that the X-mode wave does not affect the signal at the receivers and will further strengthen confidence in the feasibility of the diagnostic.

Further improvements could include extension to 3D, inclusion of the full details of the tokamak magnetic field topology and a more realistic antenna geometry. It is also planned to investigate the effects of toroidal ripples, density and magnetic fluctuations on reflectivity. Such realistic models will provide a basis for the interpretation of the experimental measurements.

## ACKNOWLEDGEMENTS

This work was supported in part by the U.S. Department of Energy under DE-FG02-95ER54309.

## BIBLIOGRAPHY

- <sup>1</sup>E. TFR, Nucl. Fusion **18**, 647 (1978).
- <sup>2</sup>H. Soltwisch, Plasma Phys. Controll. Fusion **34**, 1669 (1992).
- <sup>3</sup>R. Wolf, J. O'Rourke, A. Edwards, and M. V. Hellermann, Nucl. Fusion **33**, 663 (1993).
- <sup>4</sup>K. Gentle, Rev. Mod. Phys. **67**, 809 (1995).
- <sup>5</sup>A. Donné, Plasma Phys. Control. Fusion **44**, B137 (2002).
- <sup>6</sup>F. Levinton, G. Gammel, R. Kaita, H. Kugel, and D. Roberts, Rev. Sci. Instrum. **61**, 2914 (1990).
- <sup>7</sup>D. Wróblewski, K. Burrell, L. Lao, P. Politzer, and W. West, Rev. Sci. Instrum. **61**, 3552 (1990).
- <sup>8</sup>E. Mjølus, J. Plasma Phys. **31**, 7 (1984).
- <sup>9</sup>F. Volpe, Review of Scientific Instruments **81**, 10D905 (2010).
- <sup>10</sup>V. Shevchenko, M. De Bock, S. Freethy, A. Saveliev, and R. Vann, Fusion Science and Technology **59**, 663 (2011).
- <sup>11</sup>R. Vann *et al.*, Rev. Sci. Instrum. **87**, this conference (2016).
- <sup>12</sup>Y. Nagayama, D. Kawahara, T. Yoshinaga, *et al.*, Rev. Sci. Instrum. **83**, 10E305 (2012).
- <sup>13</sup>W. Lee *et al.*, Nucl. Fusion **54**, 023012 (2014).
- <sup>14</sup>C. Muscatello, C. Domier, X. Hu, *et al.*, Rev. Sci. Instrum. **85**, 11D702 (2014).
- <sup>15</sup>“COMSOL Multiphysics,” ([www.comsol.com](http://www.comsol.com)).
- <sup>16</sup>S. Shiraiwa, O. Meneghini, R. Parker, P. Bonoli, M. Garrett, M. Kaufman, J. Wright, and S. Wukitch, Physics of Plasmas **17**, 056119 (2010).
- <sup>17</sup>J. Jeong, Y. Bae, M. Cho, and W. Namkung, Korean Physical Society **49**, S201 (2006).
- <sup>18</sup>F. Volpe, *Electron Bernstein emission diagnostic of electron temperature profile at W7-AS Stellarator*, Ph.D. thesis, Max-Planck-Institut fuer Plasmaphysik, Garching (DE) (2003).